

1  
2  
3  
4  
5  
6  
7  
8  
9  
10  
11  
12  
13  
14  
15  
16  
17  
18  
19  
20

# Experimental evaluation of changes in strain under compressive fatigue loading of brick masonry

I.S. Koltsida<sup>a,1</sup>, A.K. Tomor<sup>a</sup>, C.A. Booth<sup>a</sup>

<sup>a</sup> Faculty of Environment and Technology, University of the West of England, Frenchay Campus, Coldharbour Lane, Bristol BS16 1QY, UK

<sup>1</sup> Corresponding author. Tel.: +44 (0) 1173283049. E-mail addresses: Iris.Koltsida@uwe.ac.uk.

---

## ABSTRACT

Assessing the long-term performance of masonry structures and their response to increased loading conditions are critical to safety and maintenance. A series of laboratory tests have been carried out on brick masonry to assess its performance under long-term fatigue loading. The relationship between stress levels and number of cycles to failure was identified under compressive loading, together with stress-strain evolution at various stress levels. Strain evolution shows distinctive characteristics for the three stages of deterioration and increased strain for increased number of cycles. Experimental results provide useful data for developing analytical prediction models for the fatigue deterioration of masonry structures.

*Keywords:* Brick Masonry, Fatigue, Strain Evolution, Stress-Strain curves, SN curves

---

## 21 1. Introduction

22 The longest standing bridges around the world are  
23 masonry arch bridges, representing around 40% of  
24 the highway, railway and waterway bridge  
25 infrastructure in Europe [1]. Due to their age and  
26 constantly increasing weight, speed and density of  
27 traffic, their assessment and maintenance are  
28 becoming increasingly important to ensure their  
29 continued safe performance.

30 High-cycle fatigue loading experienced over 100+  
31 years of service life can lead to significant changes  
32 on the material level and deterioration below  
33 serviceability or ultimate failure load [2].  
34 Identifying the rate of fatigue deterioration and  
35 changes in the material properties for masonry are  
36 necessary to enable improved assessment of load  
37 capacity, remaining service life, optimising traffic  
38 loading and planning maintenance works.

39 Limited data is however available for assessing the  
40 fatigue capacity of masonry structures. Some  
41 experimental data is available on SN curves (stress  
42 vs. number of cycles) for masonry under fatigue  
43 loading (Abrams *et al.*, 1985; Clark, 1994; Ronca  
44 *et al.* 2004; Roberts *et al.*, 2006; Tomor &  
45 Verstryngge, 2013; Tomor *et al.*, 2013) but minimal

46 information has been presented on the evolution of  
47 strain under fatigue deterioration.

48 Abrams *et al.* [3] performed experimental test  
49 series on brickwork prisms to investigate the  
50 mechanics of masonry under cyclic compressive  
51 stress. Abrams *et al.* concluded that cyclic loading  
52 leads to gradual reduction in the compressive  
53 strength of masonry and that the rate of reduction  
54 is a function of the mortar strength, amplitude and  
55 number of cycles. Greater cyclic stress levels and  
56 stronger mortars accelerate deterioration. Clark [4]  
57 conducted similar experiments and proposed SN  
58 curves for dry and wet masonry, suggesting a  
59 fatigue limit for dry brick masonry around ~50% of  
60 its quasi-static compressive strength.

61 Roberts *et al.* [5] defined a lower bound fatigue  
62 strength for dry, submerged and wet brick masonry  
63 based on a series of quasi-static and high cycle  
64 fatigue tests on brick masonry (Equation 1.1).

$$F(S) = \frac{(\Delta\sigma\sigma_{max})^{0.5}}{f_c} = 0.7 - 0.05 \log N \quad 1.1$$

65 Where F(S) is the function of the induced stress,  $\Delta\sigma$   
66 is the stress range,  $\sigma_{max}$  is the maximum stress,  $f_c$  is  
67 the quasi-static compressive strength of masonry  
68 and N is the number of load cycles.

69 Casas [2] proposed a probability-based fatigue  
70 model for brick masonry under compression with  
71 different defined confidence levels based on the  
72 experimental data reported by Roberts *et al.* [5]  
73 (Equation 1.2).

$$S_{max} = A \times N^{-B(1-R)} \quad 1.2$$

74 Where  $S_{max}$  is the ratio of the maximum loading  
75 stress to the quasi-static compressive strength, N is  
76 the number of cycles to failure and R is the ratio of  
77 the minimum stress to the maximum stress  
78  $\sigma_{min}/\sigma_{max}$ . Coefficients A and B depend on the value  
79 of the survival function and were calculated by  
80 Casas [2].

81 Tomor and Verstryngge [6] proposed a joined  
82 fatigue-creep deterioration model. A probabilistic  
83 fatigue model was suggested by adapting Casas'  
84 [7] model and introducing a correction factor C,  
85 allowing the interaction between the creep and  
86 fatigue phenomena to be taken into account and  
87 adjusting the slope of the SN curve (Equation 1.3).

$$S_{max} = A \cdot N^{-B(1-C \cdot R)} \quad 1.3$$

88 Where  $S_{max}$  is the ratio of the maximum stress to  
89 the average compressive strength ( $S_{max} = \sigma_{Max}/f_c$ ),  
90 N the number of cycles, R the ratio of the minimum

91 stress to the maximum stress ( $R = \sigma_{Min}/\sigma_{Max}$ ),  
92 parameter A is set to 1, parameter B is set to 0.04  
93 and C is the correction factor.

94 Tomor and Verstryngge [6] identified three stages of  
95 fatigue deterioration with the use of an acoustic  
96 emission technique to monitor the response of  
97 masonry prisms under long-term fatigue in  
98 compression. During the first stage (0-75% of the  
99 total number of cycles), the acoustic emission  
100 levels were relatively low and constant. A small  
101 increase in emission was observed in the second  
102 stage (75-95% cycles), followed by rapid increase  
103 in emission and sudden failure during the third  
104 stage (95-100% cycles).

105 Tomor *et al.* [8] also identified three distinct stages  
106 of fatigue deterioration based on acoustic emission  
107 levels. During Stage I, reduction in emission was  
108 observed (0-32% of the total loading cycles for  
109 compression and 0-58% for shear). During Stage  
110 II, emission stabilised (32-67% for compression,  
111 not evident in shear) and in Stage III rapid increase  
112 in emission was observed, leading to failure (67-  
113 100% for compression, 58-100% shear).

114 Carpinteri *et al.* [9] performed a series of quasi-  
115 static and cyclic tests (8 specimens tested at 70%

116 stress) on brick masonry specimens and walls and  
 117 suggested a  $\varepsilon$ -N curve (strain vs. number of cycles)  
 118 with three distinctive stages. During Stage I  
 119 deformations increased rapidly for the first 10% of  
 120 loading cycles, during Stage II deformations  
 121 increased at a constant rate (10-80% of loading  
 122 cycles) and during Stage III deformations increased  
 123 rapidly again, leading to failure. Carpinteri *et al.*  
 124 [9] also related the rate of change in vertical  
 125 deformation during Stage II ( $\partial\varepsilon_v/\partial n$ ) to the number  
 126 of cycles at failure ( $N_f$  cycles) as shown in Equation  
 127 1.4.

$$N_f = a \left( \frac{\partial\varepsilon_v}{\partial n} \right)^b \quad 1.4$$

128 Where  $\varepsilon_v$  is the vertical deformation, n is the  
 129 number of cycles and  $N_f$  is the number of loading  
 130 cycles at failure. Parameters  $a$  and  $b$  are material  
 131 constants, that can be evaluated experimentally by  
 132 applying a number of loading cycles on a prism up  
 133 to the point here deformation starts to increase at a  
 134 constant rate (over 10% of the fatigue life).

135 There are conflicting results for the different stages  
 136 of fatigue for masonry and a lack of experimental  
 137 data for identifying appropriate SN curves for  
 138 different types of masonry and the evolution of  
 139 strain under fatigue loading. The aim of this study

140 is to i) investigate the stages of fatigue  
 141 deterioration, ii) investigate the evolution of strain  
 142 and stress-strain curves and iii) provide test data to  
 143 develop mathematical models to predict the fatigue  
 144 life of masonry.

## 146 2. Quasi-static and long-term cyclic tests 147 under compression

148 Based on the work of Roberts *et al.* [5] and Tomor  
 149 *et al.* [8], a series of brick masonry prisms have  
 150 been tested under quasi-static and long-term cyclic  
 151 compressive loading to identify changes in the  
 152 material properties of masonry.

### 153 2.1 Materials

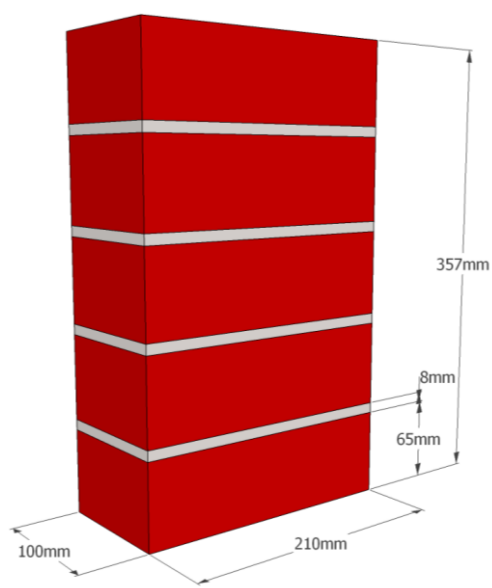
154 The experimental study intends to represent the  
 155 weakest form of masonry, widely found in the UK  
 156 waterways network, originating from the 1750s-  
 157 1850s. Brick masonry prisms were built using  
 158 handmade low-strength solid 210x100x65 mm<sup>3</sup>  
 159 Michelmersh bricks (B1 bricks). The average  
 160 compressive strength of the bricks was 4.86 N/mm<sup>2</sup>  
 161 (1.19 N/mm<sup>2</sup> standard deviation (SD) and 24.48%  
 162 coefficient of variation) and the gross dry density  
 163 1823 kg/m<sup>3</sup>. Lime-mortar with 0:1:2 cement: lime:  
 164 sand by volume (M01 mortar) was used with

165 NHL3.5 lime and 3 mm sharp washed sand and the  
166 mortar joints were 8 mm thick.

## 167 2.2 Test specimens

168 Small-scale masonry prisms (B1M01) comprised  
169 of five stack-bonded bricks with four 8 mm mortar  
170 joints built according to the ASTM standards  
171 (ASTM, 2014) with total dimensions of 210 x 100  
172 x 357 mm<sup>3</sup> (Figure 2-1). In order to have systematic  
173 building quality, the same experienced master  
174 stonemason constructed all specimens.

175 Specimens were cured at room temperature for a  
176 minimum of five days, stored outdoors for a  
177 maximum of six months and acclimatised for a  
178 minimum of three days at room temperature prior  
179 to testing (Oliveira *et al.*, 2006).

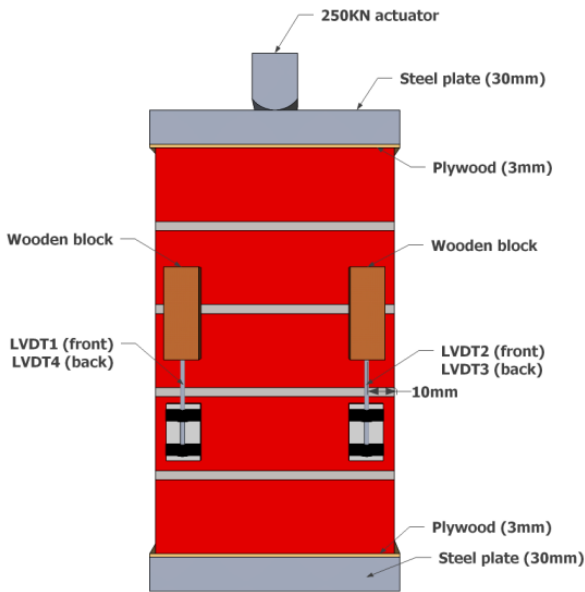


180

181 **Figure 2-1** Masonry prism dimensions

## 182 2.3 Test setup, preparation and instrumentation

183 Specimens were tested under compression using a  
184 250 kN actuator. Deflections were monitored using  
185 four Linear Variable Differential Transformers  
186 (LVDTs) with  $\pm 5$  mm linear range and 0.07%  
187 accuracy. Two LVDTs were attached at the front  
188 and two in the back of the prisms (Figure 2-2).  
189 LVDTs were positioned at 10 mm distance from  
190 the edges of the prisms and set against wooden  
191 blocks (Tomor & Verstrynge, 2013; Tomor *et al.*,  
192 2013). The distance between the wooden blocks  
193 and the LVDTs was ca. 81 mm and included two  
194 mortar joints (8 mm each) and one brick (65 mm).  
195 The upper and lower surfaces of the prisms were  
196 brushed to remove loose particles and ground flat  
197 prior to the test (Oliveira *et al.*, 2006; ASTM,  
198 2014). Prisms were placed, subsequently, between  
199 layers of 3 mm plywood and 30 mm steel plates to  
200 ensure effective load distribution and to reduce  
201 localised stress concentrations (Tomor &  
202 Verstrynge, 2013; Tomor *et al.*, 2013).



203  
204 **Figure 2-2** Instrumentation of prisms

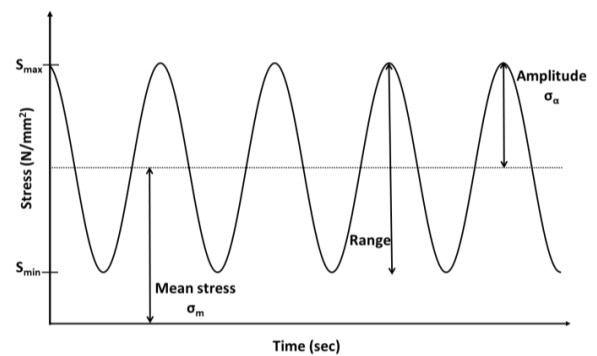
205  
206 **2.4 Loading**

207 Three sets of tests were performed under quasi-  
208 static and fatigue loading to identify material  
209 properties and to investigate changes in the  
210 material during high-cycle compressive fatigue  
211 loading of masonry prisms.

212 • Quasi-Static tests. A set of six prisms were  
213 tested under displacement-controlled quasi-static  
214 compression to obtain the mean compressive  
215 strength of the material. Loading was applied at  
216 0.01 mm/sec rate of displacement to obtain the full  
217 stress-strain curve.

218 • Fatigue tests - Type I. Masonry prisms  
219 were tested under long-term compressive cyclic  
220 loading at 2 Hz frequency to identify the number of

221 cycles to failure at different stress levels. Before  
222 the start of the fatigue tests, quasi-static loading  
223 was applied up to the mean fatigue load. Fatigue  
224 loading was subsequently applied in a sinusoidal  
225 pattern (Figure 2-3), between defined minimum  
226 and maximum stress levels.

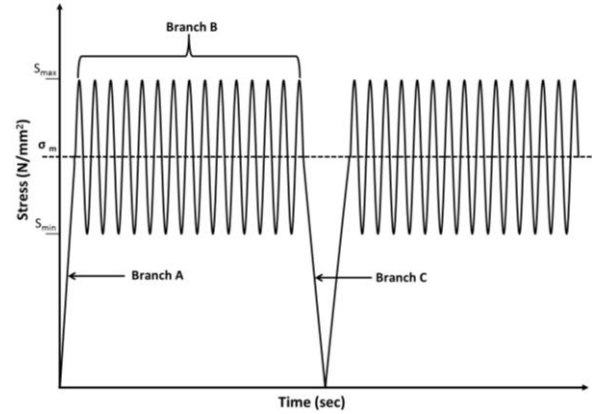


227  
228 **Figure 2-3** Sinusoidal load pattern for Type I fatigue tests

229 The minimum ( $S_{min}$ ) and maximum ( $S_{max}$ ) stress  
230 levels were expressed as percentage of the mean  
231 ultimate quasi-static strength. The minimum stress  
232 represent the dead load of the structure due to its  
233 self-weight and was set to 10% of the ultimate  
234 compressive strength to enable the most extreme  
235 range of fatigue loading to be applied.

236 The maximum stress level represents live load (e.g.  
237 similar to traffic over a masonry arch bridge) and  
238 ranged between 55% and 80% (55%, 60%, 68%,  
239 80%) of the ultimate compressive strength for the  
240 individual specimens.

241 • Fatigue tests - Type II. The second set of  
 242 fatigue tests was designed to identify stages during  
 243 fatigue deterioration and evolution of the stress-  
 244 strain curves. Loading was first applied statically  
 245 up to the mean fatigue stress level  $\sigma_m$  under  
 246 displacement control at a 0.01 mm/sec loading rate  
 247 (Branch A, Figure 2-4), cycled sinusoidally  
 248 between the minimum and maximum load levels  
 249 for 1000 cycles (Branch B, Figure 2-4) and  
 250 unloaded (Branch C, Figure 2-4). The process was  
 251 repeated until failure occurred. Branch A was used  
 252 to identify the stress-strain relationship, up to the  
 253 mean fatigue stress level, every 1000 cycles during  
 254 the fatigue life of the prisms. Similarly to Type I  
 255 fatigue tests, the minimum stress level was set to  
 256 10% of the compressive strength and the maximum  
 257 stress level was set to 63%, 68% and 73% for the  
 258 individual specimens.



259

260 **Figure 2-4** Load pattern for Type II fatigue tests  
 261 (Branch A quasi-static loading, Branch B cyclic loading,  
 262 Branch C unloading)

263

### 264 **3. Results**

#### 265 *3.1 Quasi-static tests*

266 The mean compressive strength for the set of  
 267 B1M01 prisms tested, according to BS EN 1052-  
 268 1:1999, was 2.94 N/mm<sup>2</sup> (SD 0.10 N/mm<sup>2</sup>). During  
 269 quasi-static compression vertical cracks developed  
 270 initially around the middle of the specimens and  
 271 subsequently on the narrow sides, leading to failure  
 272 (Figure 3-1).

#### 273 *3.2 Fatigue Tests – Type I.*

274 A total of 32 prisms were tested to failure under  
 275 maximum stress levels of 55, 60, 68 or 80% of the  
 276 average quasi-static compressive strength (see  
 277 section 2.4). The maximum number of loading  
 278 cycles was recorded and shown in Table 3-1.

279 **Table 3-1** Fatigue test results - Type I

Specimen Name	Load range (kN)	Stress Range (N/mm <sup>2</sup> )	N	Specimen Name	Load range (kN)	Stress Range (N/mm <sup>2</sup> )	N
B1M01-18	6-49	0.29-2.33	2,566	B1M01-57	6-42	0.29-2.00	1,100
B1M01-48	6-49	0.29-2.33	14,073	B1M01-26	6-37	0.29-1.76	25,342
B1M01-49	6-49	0.29-2.33	2,832	B1M01-28	6-37	0.29-1.76	2,646,302
B1M01-50	6-49	0.29-2.33	456	B1M01-29	6-37	0.29-1.76	122,762
B1M01-19	6-42	0.29-2.00	1,800	B1M01-30	6-37	0.29-1.76	1,268,627
B1M01-20	6-42	0.29-2.00	3,600	B1M01-31	6-37	0.29-1.76	3,528,118
B1M01-21	6-42	0.29-2.00	13,000	B1M01-32	6-37	0.29-1.76	986,325
B1M01-22	6-42	0.29-2.00	17,350	B1M01-33	6-37	0.29-1.76	796,744
B1M01-23	6-42	0.29-2.00	18,651	B1M01-34	6-34	0.29-1.62	56,562
B1M01-24	6-42	0.29-2.00	18,276	B1M01-40	6-34	0.29-1.62	412,774
B1M01-35	6-42	0.29-2.00	3,000	B1M01-41	6-34	0.29-1.62	1,088,560
B1M01-36	6-42	0.29-2.00	6,737	B1M01-43	6-34	0.29-1.62	2,200
B1M01-53	6-42	0.29-2.00	134	B1M01-44	6-34	0.29-1.62	4,864
B1M01-54	6-42	0.29-2.00	3,541	B1M01-45*	6-34	0.29-1.62	10,225,676
B1M01-55	6-42	0.29-2.00	5,994	B1M01-46	6-34	0.29-1.62	1,724,587
B1M01-56	6-42	0.29-2.00	212	B1M01-47	6-34	0.29-1.62	1,672,237

\* No failure, testing discontinued

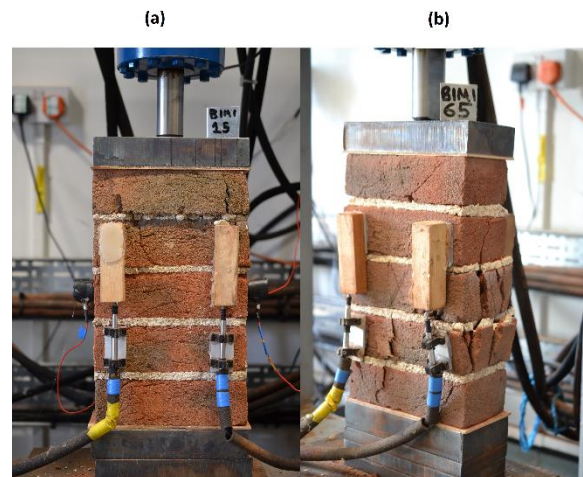
280

281 The failure patterns under fatigue loading were  
 282 very similar to quasi-static loading with vertical  
 283 splitting cracks along the middle of the specimens,  
 284 leading to failure (Figure 3-1).

285 Results of the quasi-static and fatigue compression  
 286 tests are shown in Figure 3-2 together with  
 287 proposed SN relationships by Casas [2] and Tomor  
 288 & Verstryngge [6]. Quasi-static test results are  
 289 included as failure at 1 cycle. The SN relationship  
 290 by Casas [2] gives a good indication of the mean  
 291 number of cycles at each stress level, while the  
 292 relationship by Tomor and Verstryngge [6]

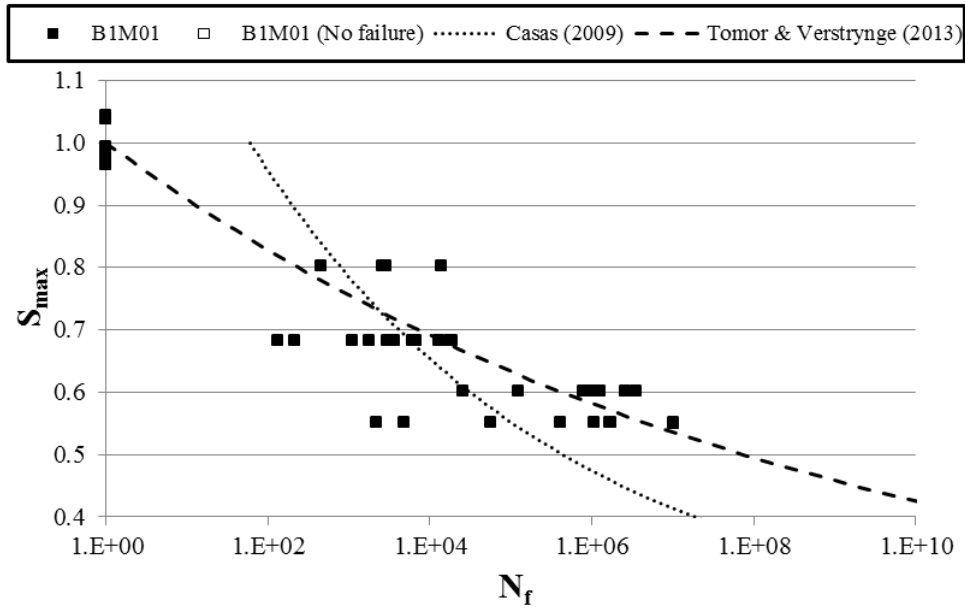
293 incorporates the quasi-static test results, although  
 294 slightly overestimates the mean number of cycles.

295



296 **Figure 3-1** Typical failure pattern under (a) quasi-static  
 297 compression and (b) fatigue compression





298

299 **Figure 3-2** Fatigue test data together with SN curves [2, 6].

300 During the Type I Fatigue tests, maximum and  
 301 minimum total longitudinal displacements were  
 302 recorded and the strain evolution curves ( $\varepsilon$ - $N/N_f$ )  
 303 plotted for each stress level in Figure 3-3 to Figure  
 304 3-6 (for 55, 60, 68, 80% maximum stress  
 305 respectively). The  $\varepsilon$ - $N$  curves exhibit a typical S  
 306 shape (Holmen, 1982; Carpinteri *et al.*, 2014), with  
 307 three distinct stages:

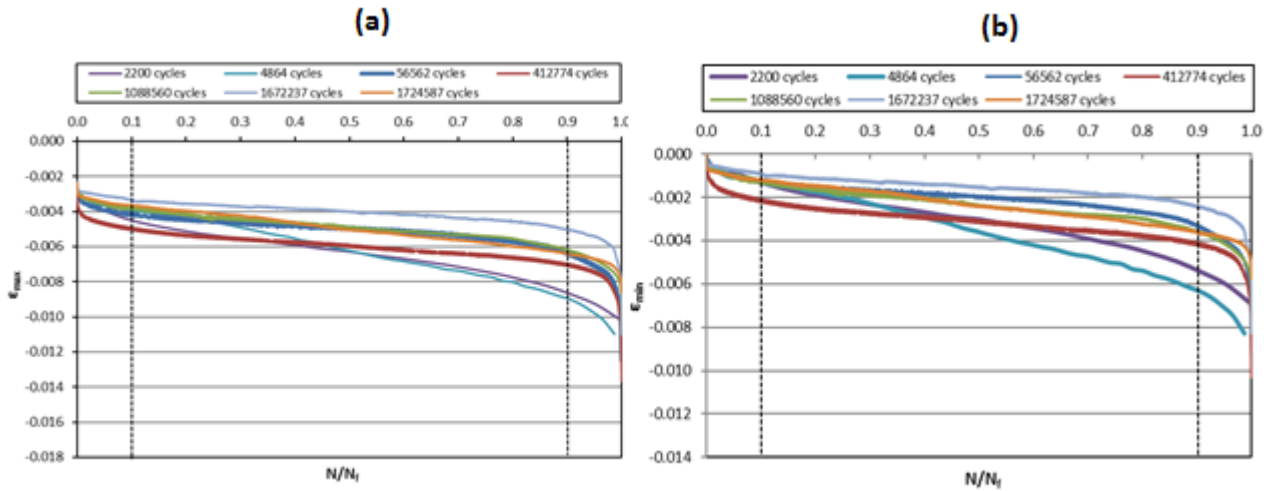
308 **Stage I:** rapid increase of strain during the first  
 309 10% of the life expectancy, caused by initiation of  
 310 micro-cracks.

311 **Stage II:** reveals a gradual increase of strain for  
 312 approximately 80% of the total number of cycles,  
 313 caused by development of micro-cracks.

314 **Stage III:** rapid increase of strain during the last  
 315 10-20% of life expectancy, caused by coalition of  
 316 micro-cracks into macro-cracks and leading to  
 317 failure.

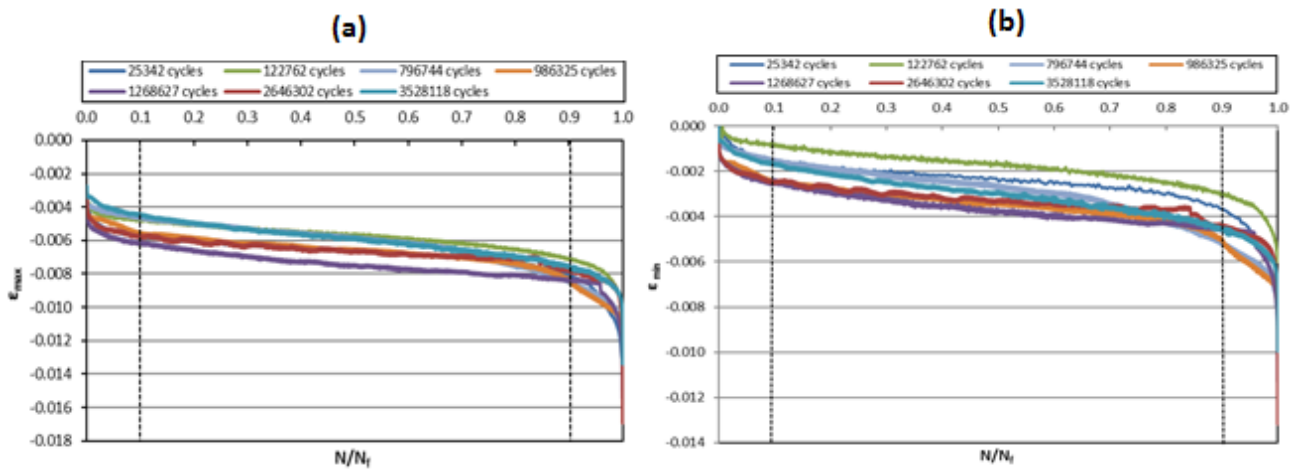
318 Carpinteri *et al.* [9] indicated that Stage II lasts  
 319 until 80% of the fatigue life of masonry based on  
 320 limited tests under 70% stress, while according to  
 321 the data presented here, Stage II occupies the range  
 322 between 10% and 90% of the total loading cycles  
 323 sustained by a prism at different stress levels.  
 324 Carpinteri *et al.* [9] proposed the use of equation  
 325 1.4 to correlate the vertical deformation with the  
 326 number of cycles. The strain evolution could be  
 327 more precisely described by three distinct  
 328 equations (parabolic type for stage I and Stage III

329 and linear type for stage II) for the different fatigue  
 330 stages that would consider the effect of stress level.

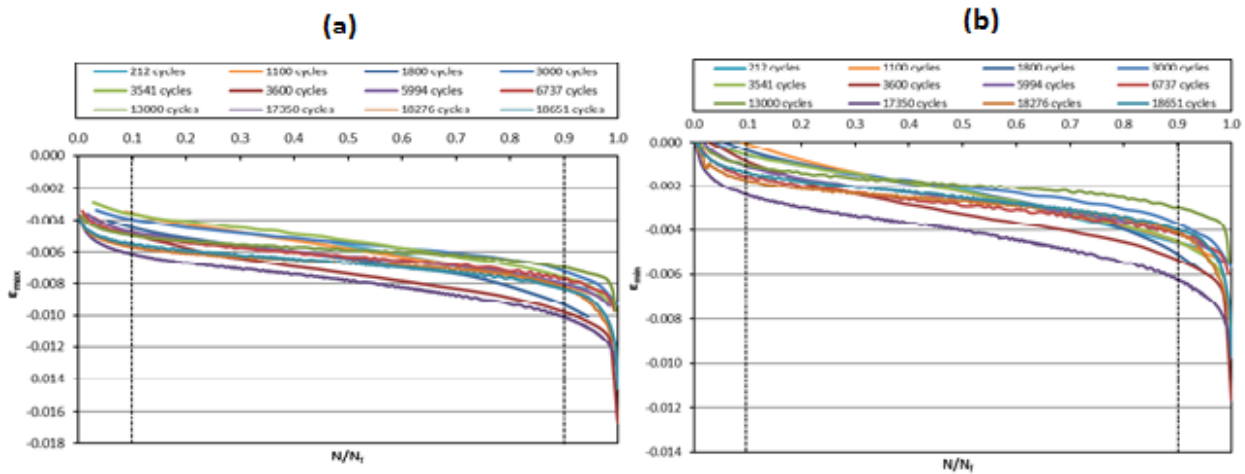


331  
 332 **Figure 3-3** Total longitudinal strain variation with the cycle ratio for 55% maximum stress level (a) maximum total strain,  
 333 (b) minimum total strain

334



335  
 336 **Figure 3-4** Total longitudinal strain variation with the cycle ratio for 60% maximum stress level (a) maximum total strain,  
 337 (b) minimum total strain

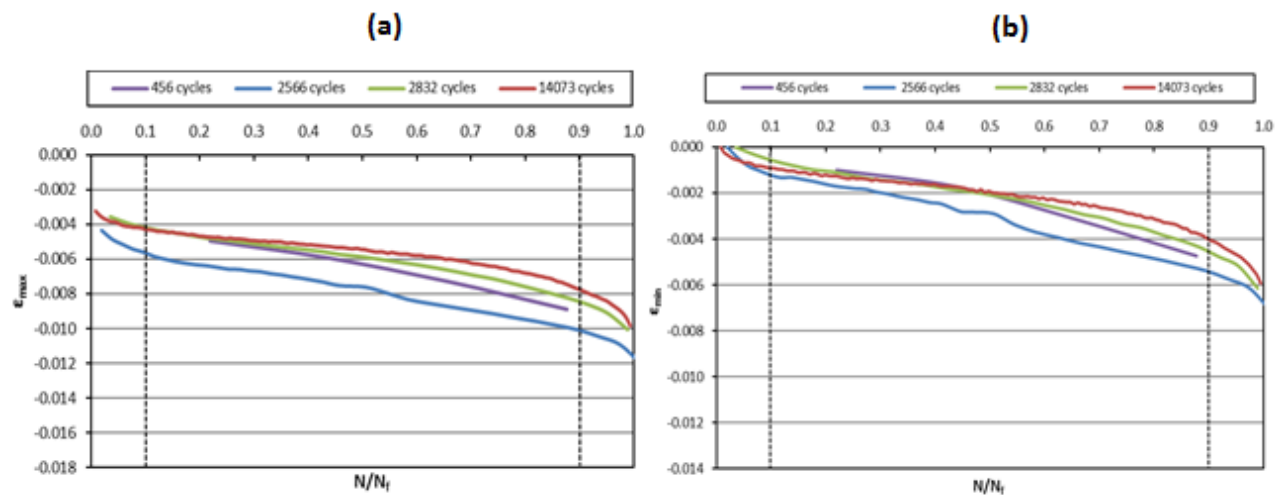


338

339 **Figure 3-5** Total longitudinal strain variation with the cycle ratio for 68% maximum stress level (a) maximum total strain,

340 (b) minimum total strain

341



342

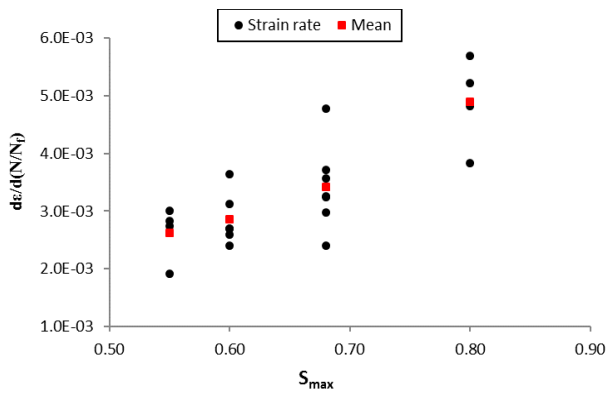
343 **Figure 3-6** Total longitudinal strain variation with the cycle ratio for 80% maximum stress level (a) maximum total strain,

344 (b) minimum total strain

345 Three stages of strain development have already  
 346 been identified in concrete under fatigue loading  
 347 (Holmen, 1982; Kim & Kim, 1996; Breitenbucher  
 348 & Ibuk, 2006; Zanuy *et al.*, 2011) and also for  
 349 masonry (Carpinteri *et al.*, 2014).

350 The rate of strain evolution at Stage II is noticeably  
 351 steeper for higher stress levels (as shown in Figure  
 352 3-7 for maximum stress levels 55%, 60%, 68% and  
 353 80%). This indicates a faster rate of the fatigue

354 process at higher stress levels leading to earlier  
 355 failure of the specimen.



356  
 357 **Figure 3-7** Strain rate ( $d\epsilon/d(N/N_f)$ ) for 55%, 60%, 68%,  
 358 80% maximum stress during Stage II Fatigue test - Type  
 359 I

360 *3.3 Fatigue tests – Type II*

361 Masonry prisms were tested under 73%, 68% and  
 362 63% maximum compressive stress during Type II  
 363 fatigue tests (see Section 2.4) and results listed in  
 364 Table 3-2 to Table 3-4.

365 **Table 3-2** Fatigue test results - Type II, 73% maximum  
 366 stress

Specimen Name	Load Range (kN)	Stress Range (N/mm <sup>2</sup> )	N
B1M01-66	6-45	0.29-2.14	253
B1M01-67	6-45	0.29-2.14	200
B1M01-68	6-45	0.29-2.14	413
B1M01-69	6-45	0.29-2.14	53
B1M01-70	6-45	0.29-2.14	55
B1M01-76	6-45	0.29-2.14	7
B1M01-77	6-45	0.29-2.14	104
B1M01-78	6-45	0.29-2.14	240
B1M01-85	6-45	0.29-2.14	93

367

368 **Table 3-3** Fatigue test results - Type II, 68% maximum  
 369 stress

Specimen Name	Load Range (kN)	Stress Range (N/mm <sup>2</sup> )	N
B1M01-58	6-42	0.29-2.00	31,000
B1M01-59	6-42	0.29-2.00	69,537
B1M01-60	6-42	0.29-2.00	34
B1M01-61	6-42	0.29-2.00	71,342
B1M01-62	6-42	0.29-2.00	11,754
B1M01-63	6-42	0.29-2.00	37,938
B1M01-64	6-42	0.29-2.00	33,752
B1M01-65	6-42	0.29-2.00	275,000

370

371

372 **Table 3-4** Fatigue test results - Type II, 63% maximum  
 373 stress

Specimen Name	Load Range (kN)	Stress Range (N/mm <sup>2</sup> )	Number of cycles
B1M01-71	6-39	0.29-1.86	718
B1M01-72	6-39	0.29-1.86	11,038
B1M01-73	6-39	0.29-1.86	269
B1M01-74	6-39	0.29-1.86	2,515
B1M01-75	6-39	0.29-1.86	1,104
B1M01-79	6-39	0.29-1.86	266
B1M01-80	6-39	0.29-1.86	19,203
B1M01-81	6-39	0.29-1.86	54
B1M01-82	6-39	0.29-1.86	34,728
B1M01-83	6-39	0.29-1.86	3,355
B1M01-84	6-39	0.29-1.86	256
B1M01-86	6-39	0.29-1.86	59,921
B1M01-87	6-39	0.29-1.86	543
B1M01-88	6-39	0.29-1.86	4,809
B1M01-89	6-39	0.29-1.86	881

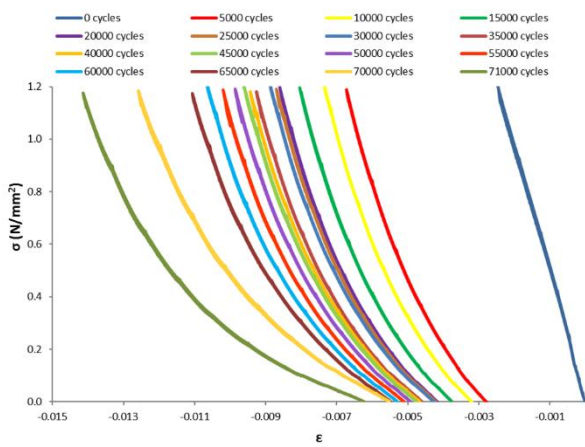
374

375

376 Evolution of the stress-strain curves for 68% and  
 377 63% maximum stress identified every 1000 cycles

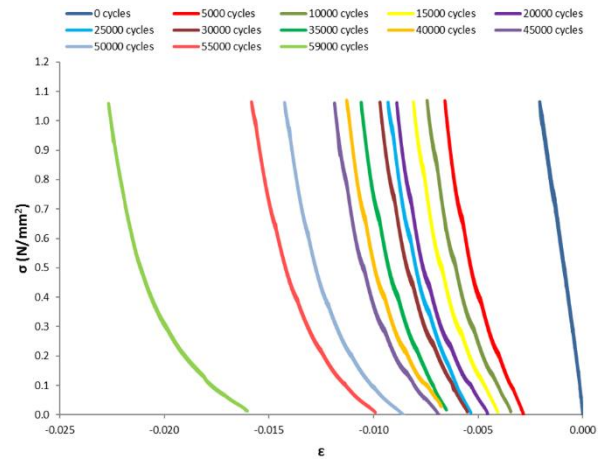
378 (every 500 cycles for BIM01-83 and BIM01-88)  
 379 are shown in Figure 3-8 and Figure 3-9. No stress-  
 380 strain curve could be identified for 73% stress due  
 381 to rapid deterioration and failure under 300 cycles.  
 382 The stress-strain curve is straight initially (or  
 383 slightly concave towards the strain axis) and  
 384 becomes convex and increasingly curved for  
 385 increasing load cycles. The residual strain is large  
 386 in Stage I, decreases and stabilises in Stage II and  
 387 increases fast again in Stage III. Concrete exhibits  
 388 similar behaviour under fatigue loading [10, 11].

389



390

391 **Figure 3-8** Stress-strain curve development every 1000  
 392 cycles under 68% maximum stress (BIM01-61)



393

394 **Figure 3-9** Stress-Strain curve development every 1000 cycles  
 395 under 63% maximum stress (BIM01-86)

396 It is noteworthy that the maximum recorded strains  
 397 at failure, during quasi-static compressive tests are  
 398 noticeably lower compared to respective strains  
 399 under fatigue loading. Thus, prior cyclic loading of  
 400 a masonry prism imposes additional deformation.

401 The maximum strain at failure is the lowest under  
 402 quasi-static loading (0.002-0.005; mean 0.003; SD  
 403 0.001) and increases for lower fatigue stress levels  
 404 (0.005-0.018; mean 0.012; SD 0.005 for 68%  
 405 maximum stress and 0.017-0.025; mean 0.020; SD  
 406 0.003 for 63% maximum stress). Increased strain  
 407 under lower fatigue stress levels is likely to be  
 408 associated with increasing effect of creep. For  
 409 extended test durations creep damage is  
 410 accumulated during the relatively longer time spent  
 411 near the peak stress of each cycle.

412 **4. Discussion**

413 Masonry arch bridges are subjected to increasing  
414 traffic loading and gradual material deterioration  
415 due to environmental impact and fatigue loading.  
416 Changes in the material properties have direct  
417 influence on the load carrying capacity and rate of  
418 deterioration of the overall structure. Very little  
419 guidance is, however, available for estimating  
420 changes in the material properties for masonry over  
421 time. Test data will next be used to develop  
422 mathematical models for the evolution of material  
423 properties under fatigue compressive loading.  
424 Mathematical models can in turn be used for  
425 improved modelling of masonry under changing  
426 load regimes and estimating the load-carrying  
427 capacity over time to improve assessment,  
428 maintenance and restoration masonry arch bridges.

429 The fatigue life of the structure can be evaluated by  
430 available SN models [2, 6]. Past and future loading  
431 history may be estimated using simplified load  
432 models, e.g. Miner’s Rule (Equation 4.1) [12] to  
433 evaluate the residual service life.

$$\frac{n_1}{N_1} + \dots + \frac{n_{i-1}}{N_{i-1}} + \frac{n_i}{N_i} < 1 \quad 4.1$$

434 Where  $n_i$  is the number of cycles at any stress range  
435 and  $N_i$  is the number of cycles causing failure at  
436 the corresponding stress range. Knowing the  
437 number of cycles that the structure has experienced  
438 an appropriate stress-strain curve can be selected  
439 for the assessment of a masonry arch bridge (e.g.  
440 using finite element models).

441 Changes in the deformability of a masonry arc  
442 bridge under traffic loading, observed during  
443 monitoring, can be associated with the  
444 experimentally recorded  $\epsilon$ -N curve configuration  
445 and contribute to appropriate maintenance  
446 planning. The configuration of the  $\epsilon$ -N curve  
447 indicates that strain changes with high rate and in  
448 parabolic shape during stage I and III and linearly  
449 at a constant rate during the second stage. An  
450 observed sudden change during long-term  
451 monitoring of a structure from linear growth of  
452 strain to a non-linear trend could mean that the  
453 structure is undergoing stage III and major  
454 strengthening is required or traffic needs to be  
455 diverted.

456

## 457 **5. Conclusions**

458 This study presents test results from small-scale  
459 laboratory tests on changes of the material  
460 properties of masonry under compressive fatigue  
461 loading.

462 Strain evolution curves ( $\epsilon$ - $N$ ) exhibit a typical ‘S’  
463 configuration with three distinct stages. During the  
464 first stage (10% of  $N_f$ ), strains grow rapidly  
465 indicating initiation of micro-cracks. Stage II is the  
466 dominant stage (10-90% of  $N_f$ ) during which the  
467 strains grow steadily until Stage III (90-100% of  
468  $N_f$ ), at which point, coalition of micro-cracks to  
469 macro-cracks leads to sudden failure of the prism.  
470 The rate of strain evolution in Stage II of the fatigue  
471 life is lower for lower stress levels.

472 The configuration of the stress-strain curve  
473 changes during cyclic compressive loading from  
474 concave with respect to the strain axis to convex  
475 with greater curvature for increased loading cycles.  
476 Large initial change in the residual strain is  
477 observed in Stage I, reduced and relatively constant  
478 strain in Stage II and increases again in Stage III.

479 Prior cyclic loading of masonry imposes additional  
480 deformation. The maximum strain at failure is  
481 greater for lower fatigue stress levels, likely to be  
482 due to the effect of creep for longer test durations.

483 Test data will be used to develop probability based  
484 mathematical models for the evolution of material  
485 properties under fatigue compressive loading.  
486 Improved models for material properties will  
487 enable enhanced modelling of masonry arch  
488 bridges and estimation of the load carrying  
489 capacity and remaining service life over time.

## 491 **Acknowledgement**

492 The work reported in this paper was supported by  
493 the International Union of Railways (UIC). The  
494 technical and financial support provided, is  
495 gratefully acknowledged by the authors.

## 496 **References**

- [1] S. Sustainable Bridges Project, “European Railway Bridge Demography, Deliverable D1.2 – Technical report,” 2004.
- [2] J. R. Casas, “A probabilistic fatigue strength model for brick masonry under compression,” *Construction and Building Materials*, vol. 23, no. 8, pp. 2964-2972, 2009.
- [3] D. P. Abrams, J. L. Noland and R. H. Atkinson, “Response of Clay-unit Masonry to Repeated Compressive Forces,” Melbourne, Australia, 1985.
- [4] G. Clark, “Bridge Analysis Testing and Cost Causation Project: Serviceability of Brick

- Masonry,” British Rail Research Report No. LR-CES-151, 1994.
- [5] T. Roberts, T. Hughes, V. Dandamudi and B. Bell, “Quasi-static and high cycle fatigue strength of brick masonry,” *Construction and Building Materials*, vol. 20, no. 9, pp. 603-614, 2006.
- [6] A. Tomor and E. Verstryngge, “A joint fatigue–creep deterioration model for masonry with acoustic emission based damage assessment,” *Construction and Building Materials*, vol. 43, no. 1, pp. 575-588, 2013.
- [7] J. R. Casas, “Reliability-based assessment of masonry arch bridges,” *Construction and Building Materials*, vol. 25, no. 4, pp. 1621-1631, 2011.
- [8] A. Tomor, S. De Santis and J. Wang, “Fatigue deterioration process of brick masonry,” *Journal of the International Masonry Society*, vol. 26, no. 2, pp. 41-48, 2013.
- [9] A. Carpinteri, A. Grazzini, G. Lacidogna and A. Manuello, “Durability evaluation of reinforced masonry by fatigue tests and acoustic emission technique,” *Structural Control and Health Monitoring*, vol. 21, no. 6, pp. 950-961, 2014.
- [10] J. Crumley and W. Kennedy, “Fatigue and Repeated-load Elastic Characteristics of Inservice Portland Cement Concrete,” Center of highway research, The University of Texas, Texas, USA, 1977.
- [11] J. O. Holmen, “Fatigue of concrete by constant and variable amplitude loading,” *ACI*, vol. 75, no. 0, pp. 71-110, 1982. 497  
498
- [12] M. Miner, “Cumulative damage in fatigue,” *Journal of Applied Mechanics*, vol. 67, pp. A159-A164, 1945.
- [13] D. V. Oliveira, P. B. Lourenço and P. Roca, “Cyclic behaviour of stone and brick masonry under uniaxial compressive loading,” *Materials and Structures*, vol. 39, no. 2, pp. 247-257, 2006.
- [14] P. Ronca, A. Franchi and P. Crespi, “Structural failure of historic buildings: masonry fatigue tests for an interpretation model,” *Structural Analysis of Historical Constructions*, vol. 2, no. 1, pp. 273-279, 2004.
- [15] C. Zanuy, L. Albajar and P. de la Fuente, “The fatigue process of concrete and its structural influence,” *Materiales de Construcción*, vol. 61, no. 303, pp. 385-399, 2011.
- [16] ASTM, “Standard test method for compressive strength of masonry prisms,” in *Annual Book of ASTM Standards*, vol. 4.05, ASTM, Ed., West Conshohocken, ASTM International, 2014, pp. 889-895.
- [17] R. Breitenbucher and H. Ibuk, “Experimentally based investigations on the degradation-process of concrete under cyclic loading,” *Materials and Structures*, vol. 39, no. 7, pp. 717-724, 2006.
- [18] J. Kim and Y. Kim, “Experimental study of the fatigue behavior of high strength concrete,” *Cement and Concrete Research*, vol. 26, no. 10, pp. 1513-1523, 1996.